Effects of sputtering with Kr gas and insertion of lowermost layer on electrical resistivity of Ag-multilayer

Koji Mizukoshi[1,2], Takafumi Yamamura[3], Yasuhiro Tomioka[3], Midori Kawamura[2*]

[1]Manufacturing Headquarters, YKK AP Incorporated, Kurobe 938-8610, Japan
[2]Department of Materials Science and Engineering, Kitami Institute of Technology, Kitami 090-8507, Japan
[3]Technology and Innovation Center, YKK Corporation, Kurobe 938-8601, Japan

E-mail: kawamumd@mail.kitami-it.ac.jp

Silver-based low-emissivity films have been studied to improve window insulation performance. We have reduced the resistivity of Ag in glass/ZnO/Ag structures by inserting a TiO_2 in the lowermost layer. In another study, we have also found that the resistivity of Ag thin film can be reduced by changing the sputtering gas from Ar to Kr. In this study, both methods were adapted to achieve even lower resistivity and the factors involved were analyzed in detail. The lowest electrical resistivity achieved was 3.3 μΩ·cm for a combination of a glass/TiO_2/ZnO/Ag structure and Kr gas sputtering, which was 2.9% less than that for a glass/TiO_2/ZnO/Ag structure with Ar gas sputtering. X-ray diffraction, atomic force microscopy, and secondary ion mass spectroscopy results indicated that the important factor influencing the electrical resistivity was a reduction in the amount of sputtering gas trapped in the Ag layer by depositing the layer using Kr gas.

1. Introduction

Low-emissivity (Low-E) films, which were developed to improve the thermal insulation performance of windows, generally consist of a MO/Ag/MO structure, where MO indicates a metal oxide, with a 6-15 nm thick Ag layer sandwiched between the MO layers.[1-6] By coating the float glass used for window glass, an emissivity of about 0.9 of the glass becomes as low as 0.05 or less. The MO layer can consist of various transparent oxides such as TiO_2, ZnO, or SnO_2 with a thickness of 15-40 nm.[5,7] The silver layer reflects infrared rays, resulting in a glass with low emissivity. The thermal insulation performance is quantified by the emissivity, which is proportional to the sheet resistance Rs ($= \rho d^{-1}$) in the case of Low-E glass with only a single layer of silver[8, 9], where ρ is the electrical resistivity, and d is the Ag thickness. Low-E films are generally deposited using a continuous sputtering system[10], and the top and bottom MO layers are responsible for maintaining the low resistivity of the Ag layer, which has the most important effect on performance.[11] The MO layers further serve to adjust the visible light transmittance[12, 13] and to protect the Ag layer when the glass is machined or thermally processed.[14, 15]

It has been reported that Ag layers with preferential (111) orientation in the plane parallel to the substrate have lower resistivity.[16-18] We used a glass/TiO_2/ZnO/Ag structure, instead of a glass/ZnO/Ag, as the lower part of the MO/Ag/MO structure.[19] By insertion of a lowermost layer (TiO_2), the preferential orientation was promoted and the resistivity of the Ag layer was reduced by approximately 20%, compared to the glass/ZnO/Ag structure. Research has also been carried out on the effect of Ag deposition conditions such as the sputtering power[20], the sputtering gas mixture[21, 22], the use of additives to achieve high stability of the deposited Ag layer[23, 24], and use of ultrathin silver oxide interlayer.[25]

When depositing the Ag layers used in Low-E glass, Ar is generally used as the sputtering gas. In the sputtering plasma, sputtering gas ions impact the target, are electrically neutralized, collide with the target atoms and are backscattered.[26-31] These reflected atoms move toward the substrate, and the nature and properties of these atoms affect the characteristics of the deposited layer.[32, 33] The smaller the mass difference between the metal target atoms and the sputtering gas ions, the smaller the maximum energy of the reflected gas atoms becomes. For an Ag target with an atomic mass of 107.9 u, Kr with an atomic mass of 83.8 u has a smaller mass difference than Ar with an atomic mass of 40.0 u. Therefore, Kr is expected to have a smaller effect on the deposited Ag layer. West et al. deposited 500 nm thick Ag films in various inert gases and found that they were harder and smoother by sputtered with lighter inert gases. But 15 nm thick Ag film deposited on ZnO pre-coated glass showed improved properties with heavier gases.[26]

However, the process gas content was measured by energy dispersive x-ray spectroscopy and the Ar content was undetermined. In addition, although ZnO pre-coated glass was used as the substrate, no verification of ultra-thin Ag films in multilayers has been conducted. Kawamura et al. reported a reduction in the resistivity of a 150-nm-thick Ag layer by changing from Ar gas to Kr gas during the sputtering process.[27, 28] This was a result of a lower amount of sputtering gas, determined by secondary ion mass spectroscopy (SIMS), trapped in the sputtered Ag layer. However, sputtering using Kr gas has not been reported for fabricating Low-E structures. Furthermore, the effect of Kr gas sputtering on thin Ag layers with thicknesses of less than 15 nm is not clear. In the present study, we attempted to reduce the resistivity of a 14-nm-thick Ag layer using DC sputtering with Kr gas. In addition, we also studied the use of glass/TiO_2/ZnO/Ag structures, which is the lower part of MO/Ag/MO, to further reduce the resistivity with more practical multilayers.

2. Experimental methods

2.1 Specimen preparation

All samples were deposited by DC magnetron sputtering using a float-glass substrate at room temperature. The size of the substrate is 30 mm square and 3 mm thick. Before sputtering, RF plasma etching was performed under an Ar gas atmosphere. The substrate - target distance was about 60 mm. Before deposition, the process chamber was evacuated using a turbo molecular pump until the base pressure was less than 2.0×10^{-4} Pa. Figure 1 shows the structure and naming of the samples prepared in this study. As shown in Fig. 1(a), sample AG_S consisted of a single Ag layer deposited directly on glass using an Ag sputtering target (99.99%). A constant power of 2.19 $W\cdot cm^{-2}$ was used and the sputtering gas pressure was 0.2 Pa. Either Ar gas (99.99%) or Kr gas (99.999%) was used as the sputtering gas. Four different layer thicknesses of 14, 50, 100, and 150 nm were prepared by changing the deposition time. For the 100-nm-thick samples, a deposition pressure of 0.2, 0.4, 0.6, or 0.8 Pa was used. Figure 1(b) shows a schematic of the AG_D samples, which had the structure glass/ZnO/Ag. A ZnO layer with a thickness of 8 nm was first deposited using pure Zn as the metal target in an Ar/O_2 atmosphere (40% O_2) at a pressure of 0.4 Pa. An Ag layer with a thickness of 14 nm was then deposited under the same conditions used for the AG_S samples. For the AG_M samples, as shown in Fig. 1(c), the structure was glass/TiO_2/ZnO/Ag. The TiO_2 layer was deposited using pure Ti as the metal target with an Ar/O_2 atmosphere (30% O_2) at a pressure of 0.3 Pa, and a power of 6.58 $W\cdot cm^{-2}$. The thickness of the TiO_2 layer was 20 nm. The deposition conditions for the ZnO and Ag layers were the same as when preparing AG_D.

2.2 Characterization

The film thickness was evaluated using 2D step height measurements (KLA Corporation, Alpha-Step D-500) and X-ray reflectivity (XRR; Bruker D8, ADVANCE).34) The four-point probe method and eddy current method (Napson, Duoless) were used to measure the sheet resistance. The eddy current method was used only for the measurement of the Ag 14 nm thick sample for consistent comparison with previous data[19]. The surface morphology was observed with field emission scanning electron microscope (FE-SEM; Hitachi High-Tech S-4800) and atomic force microscope (AFM; Bruker, Dimension Icon) in tapping mode. To evaluate the crystal structure, out-of-plane and in-plane measurements were performed using X-ray diffraction (XRD; Rigaku, SmartLab). Using Cu Kα radiation, the crystal structure was analyzed in three XRD scanning modes: (1) out-of-plane XRD scanning (symmetric θ–2θ), which is a common measurement method for detecting crystal lattice planes parallel to the substrate surface; (2) two-dimensional XRD (2D-XRD) scanning, which is a type of out-of-plane measurement that simultaneously measures the intensity distributions in the circumferential (tilting) direction of the Debye ring and the 2θ direction, and easily detects crystal misorientations[35]; and (3) in-plane scanning, which is a method for investigating crystal planes perpendicular to the substrate surface. The composition of the Ag layer (Ar and Kr content) was measured by Rutherford backscattering spectrometry (RBS; National Electrostatics Corporation, Pelletron 3SDH) using $^{4}He^{++}$ as incident ions. The Ar concentration in the layers was quantitatively determined by dynamic secondary ion mass spectroscopy using Cs^{+} as primary ions at an accelerating voltage of 3 kV. The Kr content was analyzed qualitatively due to the lack of a standard sample.

3. Results and discussion

3.1 Effect of sputtering gas on electrical resistivity of Ag single layers

Figure 2 shows a comparison of the electrical resistivity of Ag single layers deposited in Ar and Kr gas atmospheres at different deposition pressures. The Ag layer thickness was kept constant at 100 nm, and the deposition pressure was varied from 0.2 to 0.8 Pa. For the Ag layers deposited in an Ar gas atmosphere, the average electrical resistivity was more than 2.5 μΩ·cm at all deposition pressures, and for the Ag layers deposited in a Kr gas atmosphere, it was less than 2.4 μΩ·cm. The lowest electrical resistivity was obtained at 0.6 Pa in a Kr gas atmosphere. It is noteworthy that the electrical resistivity is lower for a Kr gas atmosphere at any deposition pressure. Figure 3 shows a comparison of the electrical resistivity of Ag single-layer samples with different layer thicknesses deposited

at a pressure of 0.2 Pa in Ar and Kr gas atmospheres. The layer thicknesses are 14, 50, 100, and 150 nm. For an Ar gas atmosphere, the resistivity is 5.1 and 2.4 μΩ·cm for layer thicknesses of 14 and 150 nm, respectively. Using a Kr gas atmosphere, the resistivity was 4.8 μΩ·cm for a thickness of 14 nm, and 2.2 μΩ·cm for a thickness of 150 nm. In both gas atmospheres, the electrical resistivity decreased as the layer thickness increased, and approached the value for bulk Ag (1.62μΩ·cm at 25ºC).36) The reduction in electrical resistivity by changing from Ar to Kr gas was 5.9%, 6.9%, 8.0%, and 8.3% for thicknesses of 14, 50, 100, and 150 nm, respectively, indicating that the improvement rate increased as the layer thickness increased.

The above results indicate that the resistivity of Ag single layers deposited in a Kr gas atmosphere is lower, and this effect is also observed for a layer thickness of 14 nm. We therefore used a 14-nm-thick Ag layer in the AG_D and AG_M samples, and investigated the effects of the sputtering gas.

3.2 Effect of sputtering gas on electrical resistivity of Ag multilayer samples

Figure 4 shows the comparison of the electrical resistivity of AG_S, AG_D, and AG_M samples where the Ag layer was deposited using Ar and Kr gases. The electrical resistivity here was measured by the eddy current method. Although, the thickness of the Ag layer was constant at 14 nm for all samples, the resistivity was lower for AG_D and AG_M than for AG_S. In our previous work[17)], we investigated the use of a 20-nm-thick TiO_2 layer in a glass/TiO_2/ZnO/Ag structure, and found that this layer can reduce the electrical resistivity of the Ag layer. In that study, Ar gas was used for Ag deposition, but in the present study, the same tendency appeared when Kr gas was used, and the lowest resistivity was found for AG_M. The reduction in electrical resistivity by changing from Ar to Kr gas was 5.9%, 6.8%, and 2.9% for AG_S, AG_D, and AG_M, respectively. These results indicate that sputtering with Kr gas can reduce the resistivity of Ag multilayers used in Low-E structures.

3.3 Effect of sputtering gas on Ag surface morphology

Since the presence of a rough Ag surface and a large number of grain boundaries hinders electron transfer and increases the resistivity, the surface morphology of the Ag films was investigated. Figure 5 shows SEM images of the surfaces of Ag layers deposited using Ar and Kr gases. In both cases, the grain size ranged from a few nanometers to 500 nm. The average grain size was determined by drawing three straight lines on the SEM image and dividing the length of the line by the number of grains the line passed through. The average grain size was found to be 55 nm in the case of Ar gas and 58 nm in the case of

Kr gas. For the sample sputtered with Kr gas, the result is that the grains are about 5% larger, but did not show any significant difference.

Previous studies have shown that the surface roughness (Ra) has an important effect on electrical resistivity, with smoother surfaces leading to lower resistivity. The surface morphologies of AG_S (100 nm), AG_D, and AG_M deposited in Ar and Kr gas atmospheres were compared. AFM images of AG_S (100 nm), AG_D, and AG_M sputtered with Ar and Kr gases are shown in Fig. 6. The color scales beside the images indicate the range of surfaces heights (Z-axis). For AG_S, Ra is 1.62 nm for both sputtering gases, and there is no significant difference in the shape or size of the grains. For AG_D, Ra is 0.79 nm using Ar gas, and 0.69 nm using Kr gas. For AG_M, Ra is 0.47 nm using Ar gas, and 0.46 nm using Kr gas. Thus, the surface roughness is slightly smaller using Kr gas. In the case of AG_S and AG_M, Ra was the same for both samples sputtered with Ar and Kr. In the case of AG_D, there was a difference in the 1 μm field of view, but in the 10 μm field of view, Ra was the same at 0.66 nm for both samples sputtered with Ar and Kr. These indicate that changing the sputtering gas does not change Ra, which affects the resistivity. And, there is no difference in the shape or size of the grains. For the same Ag layer thickness, the grain size for AG_M is larger than that for AG_D. For the multilayer samples, regardless of the sputtering gas, the use of a TiO_2 layer resulted in a smaller Ra and a larger grain size. This is consistent with AG_M having a lower resistivity than AG_D.

3.4 Effect of sputtering gas on crystal orientation

In previous studies[16-18], a preferential (111) orientation for Ag layers was found to lead to lower electrical resistivity. This was thought to be because close-packed Ag planes were aligned parallel to the substrate. Figure 7 shows XRD patterns for the samples prepared in the present study. Figures 7(a) and 7(c) show out-of-plane patterns, and Figs. 7(b) and 7(d) show in-plane patterns. In Fig. 7(a) for AG_S, Ag(111) and (200) peaks are observed, and in Fig. 7(b), Ag(111), (200) and (220) peaks can be seen. In Fig. 7(a), the (111) peak intensity is strong for both sputtering gases, indicating a strong preferential (111) layer orientation parallel to the substrate. However, in Fig. 7(b), Ag(111) is observed with the same intensity as Ag(220), which indicates that Ag(111) is not sufficiently oriented preferentially in the plane parallel to the substrate. For the Ag(111) peak, whose strength is an indicator of low resistivity, no significant difference was observed between sputtering with Ar gas and sputtering with Kr gas. In the XRD pattern for AG_D shown in Fig. 7(c), peaks due to Ag(111) and ZnO(002) planes are observed. The former peak again indicates a preferential (111) orientation of the Ag layer, similar to AG_S. A similar

result is found for AG_M, but the peak intensity is higher for the latter sample, indicating that the TiO_2 layer enhances the preferred (111) orientation of the Ag layer. For AG_D, no dependence on sputtering gas was found. For AG_M, the Ag(111) peak appears slightly larger for the sample sputtered with Kr gas, but the effect is too small to be considered an effect of the sputtering gas. Similar results were also obtained from measurement of the full width at half maximum of the peaks in the 2D-XRD patterns. These results show that the highest degree of preferential Ag(111) orientation is obtained when using a TiO_2 layer and sputtering with Kr gas.

3.5 Influence of trapping of sputtering gas in Ag layer

As described in Section 3.2, the reduction in electrical resistivity by changing from Ar to Kr gas was 5.9%, 6.8%, and 2.9% for AG_S, AG_D, and AG_M, respectively. To investigate the reason for this difference, the Ar and Kr concentrations in AG_S (100 nm) layers were analyzed using RBS using $^4He^{++}$ ions. When Ar is present in the Ag layer, an Ar signal appears at 1,455 to 1,555 keV, and when Kr is present, a Kr signal appears at 1,800 to 1,910 keV. For this sample, it was found that both the concentrations of Ar and Kr were below the detection limits (about 0.1 and 0.3 at%, respectively). The samples were next subjected to a SIMS analysis. Ar and Kr contents of samples sputtered with Ar gas or Kr gas were analyzed. The results are shown in Fig. 8. For the sample sputtered with Ar gas, the concentration curve of Ar was observed, while the sample deposited with 100% Kr gas was at the background level because it did not contain Ar. Therefore, it was clear that Ar gas was trapped in the sample sputtered with Ar gas, and found to be around 8×10^{18} atoms/cm^3 (0.013 at%). But Kr content, which could be checked by intensity, was below the detection limit in both samples. In the curves of Ar and Kr in Fig. 8, there are sharp changes near the sample surface and the substrate, which are thought to be due to the mass interference caused by adsorbents on the surface and the substrate substance, respectively. The results of the present study (0.013 at% at a resistivity of 2.4 μΩ·cm) also confirm the relationship between resistivity and Ar concentration. Therefore, the amount of backscattered Ar gas is considered to be smaller for the present sputtering conditions. However, Ar was definitely present and affected the electrical resistivity. In previous studies[27], the concentration of Ar was 0.24 at% at a resistivity of 3.5 μΩ·cm, and 0.05 at% at 2.7 μΩ·cm.

Since there is no change in the lattice constants of the Ag films with different electrical resistivities, the backscattered Ar gas trapped in the film is expected to be vicinity of the grain boundaries so as to minimize the free energy of the entire system.[26] Therefore, although the concentration of 0.013% may seem low, it is believed that the Ar atoms

present at vicinity of the grain boundaries cause an increase in resistivity.
On the other hand, the Kr content was below the detection limit for both samples, likely because the backscattering energy of Kr is low due to the mass difference between Ag and Kr[26-30], and Kr was not trapped in the Ag layer. From these results, it is suggested that the lower amount of sputtering gas trapped in the Ag layer reduced the electrical resistivity.

4. Conclusions

As being found in a thick Ag films, sputtering a 14 nm thick Ag layer using Kr rather than Ar as the gas atmosphere was found to be effective at reducing the electrical resistivity of the layer. Similar effects were found for Ag multilayer structures such as AG_D and AG_M. The reduction in electrical resistivity was 6.8% for glass/ZnO/Ag and 2.9% for glass/TiO_2/ZnO/Ag, compared with the case for Ar gas. No significant differences were observed in the preferential Ag(111) orientation or the surface roughness, which generally affect the electrical resistivity. The SIMS analysis results show that the sputtering gas is not contained in the low-resistance Ag deposited using Kr gas. As a result, we have found low-e multilayer with lower resistivity can be obtained by using Kr gas that is not incorporated into the Ag film, in addition to the insertion of the lowermost layer.

References

1) R. Saidur, M. M. Hasan, A. S. M. A. Haseeb, and H. H. Masjuki, J. Appl. Sci. 8, 1883 (2008).
2) R. J Martin-Palma, R. Gago, M. Vinnichenko, and J. M Martinez-Duart, J. Phys. D: Appl. Phys. 37,1554 (2004).
3) D. R. Sahu, J.-L. Huang, Mater. Sci. Eng. B 130, 295 (2006).
4) R. J. Martin-Palma, L. Vazquez, J. M. Martinez-Duart, and Malats-Riera, Sol. Energy Mater. Sol. Cells 53, 55 (1998).
5) G. Leftheriotis, P. Yianoulis, and D. Patrikios, Thin Solid Films, 306, 92 (1997).
6) A. A. Solovyev, S. V. Rabotkin, and N. F. Kovsharov, Mater. Sci. Semicond. Process. 38 (2015). p.373.
7)B. P. Jelle, S. E. Kalnæs, and T. Gao, Energy Build. 96, 329 (2015).
8) J. Szczyrbowski, G. Bräuer, M. Ruske, H. Schilling, and A. Zmelty, Thin Solid Films

351, 254 (1999).
9) E. H. Nezhad, H. Haratizadeh, and B. M. Kari, Ceram. Int. 45, 9550 (2019).
10) R. J. Hill, S. Nadel, and M. Andreasen, in *50 Years of Vacuum Coating Technology and the Growth of the Society of Vacuum Coaters*, edited by Donald M. Mattox and Vivienne Harwood Mattox, Society of Vacuum Coaters, 2007. 2008 Summer Bulletin, p.38.
11) R. Alvarez, J. C. Gonzalez, J. P. Espinos, A. R. Gonzalez-Elipe, A. Cueva, and F. Villuendas, Appl. Surf. Sci. 268, 507 (2013).
12) Y. Tachibana, K. Kusunoki, and H. Ohsaki, Vacuum 74, 555 (2004).
13) J. H. Kim, Y. J. Moon, S. K. Kim, Y. Z. Yoo, and T. Y. Seong, Ceram. Int. 41, 14805 (2015).
14) E. Ando, M. Miyazaki, Thin Solid Films 351, 308 (1999).
15) D. C. Tasai, Z. C. Chang, B. H. Kuo, E. C. Chen, Y. L. Huang, T. J. Hsieh, and F. S. Shieu, Ceram. Int. 46, 7991 (2020).
16)K. Kato, H. Omoto, and A. Takamatsu, Vacuum 83, 606 (2009).
17) M. Arbab, Thin Solid Films 381, 15 (2001).
18)Y. Tsuda, H. Omoto, K. Tanaka, and H. Ohsaki, Thin Solid Films 502, 223 (2006).
19) K. Mizukoshi, T. Yamamura, Y. Tomioka, and M. Kawamura, Jpn. J. Appl. Phys. 60, 025501 (2021).
20) M. B. Cinali, O. D. Coskun, J. Alloys Compd. 853, 157073 (2021).
21) Y. Nakanishi, K. Kato, H. Omoto, and M. Yonekura, Thin Solid Films 532, 141 (2013).
22) J. Zhang, R. Zhang, R. Cui, J. Zhang, and Y. Pu, X. Li, Vacuum 155, 439 (2018).
23) E. Ando, S. Suzuki, N. Aomine, M. Miyazaki, and M. Tada, Vacuum 59, 792 (2000).
24) J. W. Jeong, H. Kong, H. Y. Lee, Superlattices Microstruct. 133, 106187 (2019).
25) J. Bulir, M. Novotny, A. Lynnykova, J. Lancok, Surf. Coat. Technol. 228, 051511 (2013).
26) G. T. West, P. J. Kelly, Surf. Coat. Technol. 206, 1648 (2011).
27) M. Kawamura, R. Sagara, Y. Abe, T. Kiba and K. H. Kim, Jpn. J. Appl. Phys. 59, 048001 (2020).
28) R. Sagara, M. Kawamura, T. Kiba, Y. Abe and K. H. Kim, Surf. Coat. Technol. 388, 125616 (2020).
29) Y. Takagi, Y. Sakashita, H. Toyoda, and H. Sugai, Vacuum 80, 581 (2006).
30)M. Novotny, J. Bulir, P. Pokorny, J. Lancok, L. Fekete, J. Musil, and M. Cekada, Surf. Coat. Technol. 228, S466 (2013).
31) M. Rudolph, D. Lundin, E. Foy, M. Debongnie, M.-C. Hugon, and T. Minea, Thin Solid Films 658,46 (2018).

32) C. Paturad, G. Farges, M. C. Sainte Catherine, and J. Machet, Surf. Coat. Technol. 86–87, 388 (1996).
33) P. Pokorny, J. Musil, J. Lancok, P. Fitl, M. Novotony, J. Bulir, and J. Nleck, Vacuum 143, 438 (2017).
34) K. Sakurai, M. Mizusawa, and M. Ishii, MRS-J 32 (2007).
35) K. Nagao, J. Surf. Finish. Soc. Jpn. 66 ,636 (2015) [in Japanese].
36) D. Lide, CRC Handbook of Chemistry and Physics, 84th ed., CRC, Boca Raton, FL, 2003, pp. 12–45.
37) G. Abadias, E. Chasonm J. Keckes, M. Sebastiani, G. B. Thompson, E. Barthel, G L. Doll, C. E. Murray, C. H. Stoessel, and L. Martinu, J. Vac. Sci. Technol. A 36, 020801 (2018).

Figure Captions

Fig. 1. Schematic illustrations of specimen structures (a) Ag single layer, (b) Double layer and (c) Multi-layer structure.

Fig. 2. Deposition pressure and resistivity of AG_S (100 nm) sputtered with Ar and Kr gases.

Fig. 3. Film thickness and resistivity of AG_S sputtered with Ar and Kr gases. The eddy current method and the four-point probe method are used for AG_S (14 nm) and AG_S (50, 100, 150 nm), respectively.

Fig. 4. Resistivity of AG_S (14 nm), AG_D, and AG_M sputtered with Ar and Kr gases.

Fig. 5. SEM images of AG_S (100 nm) (a) sputtered with Ar gas and (b) sputtered with Kr gas.

Fig. 6. AFM images of AG_S (100 nm), AG_D, and AG_M sputtered with Ar and Kr gases. (a) AG_S with Ar (b) AG_S with Kr, (c) AG_D with Ar, (d) AG_D with Kr, (e) AG_M with Ar, and (f) AG_M with Kr.

Fig. 7. XRD patterns for AG_S (100 nm), AG_D, and AG_M sputtered with Ar and Kr gases.
(a) and (c) out-of-plane, (b) and (d) in-plane XRD patterns.

Fig. 8. Depth profile of Ar and Kr in Ag layer measured by SIMS. (a)AG_S (100 nm) sputtered with Ar gas and (b) AG_S (100 nm) sputtered with Kr gas.

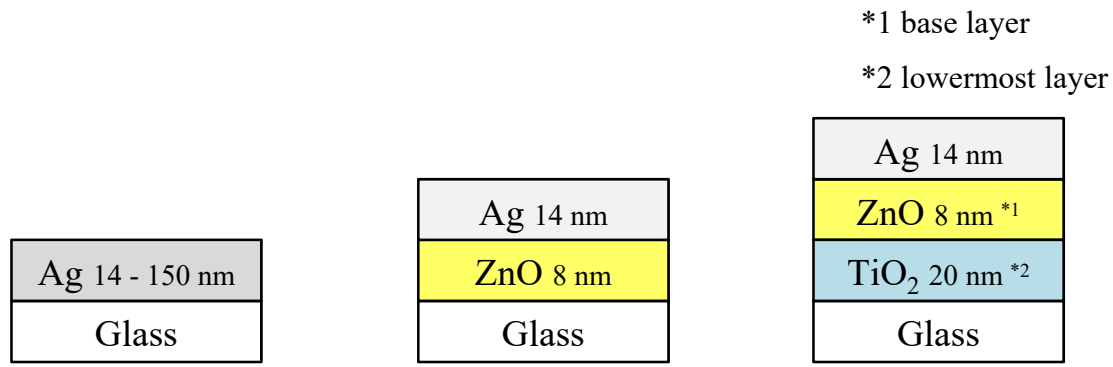

(a) Ag single layer (AG_S)

(b) Double layer (AG_D)

(c) Multi-layer (AG_M)

Fig. 1

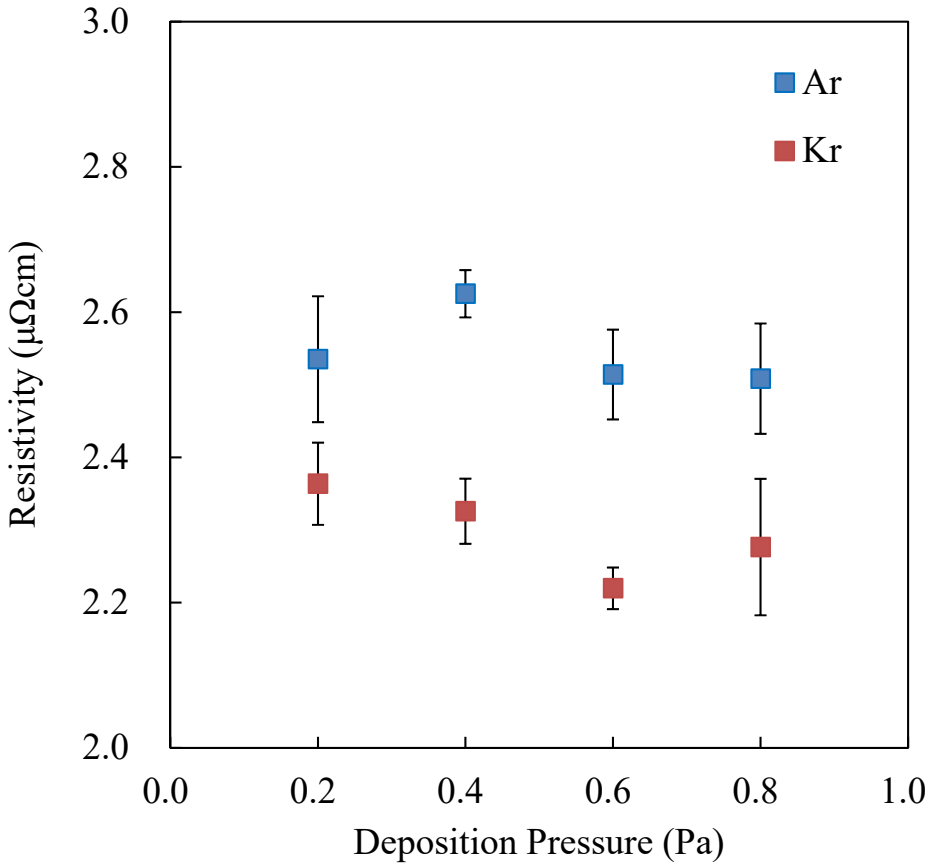
3.0
2.8
2.6
2.4
2.2
2.0
Resistivity (μΩcm)
0.0
0.2
0.4
0.6
0.8
1.0
Deposition Pressure (Pa)
Ar
Kr

Fig. 2

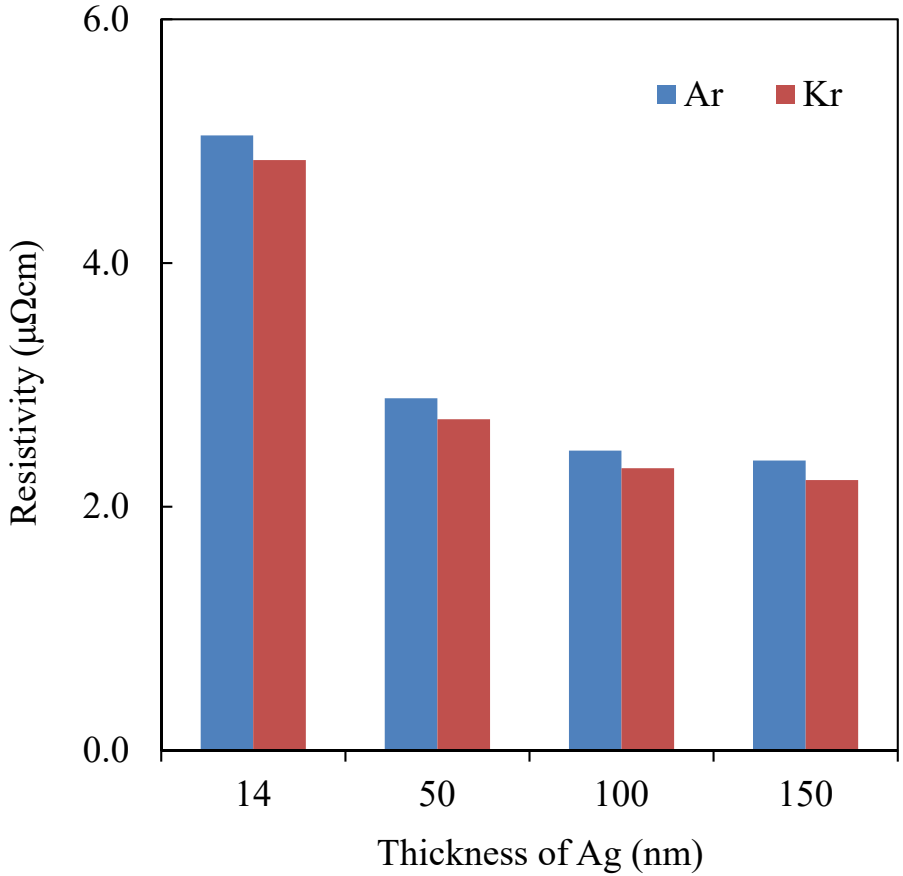
6.0
4.0
2.0
0.0
Resistivity (μΩcm)
Ar
Kr
14
50
100
150
Thickness of Ag (nm)

Fig. 3

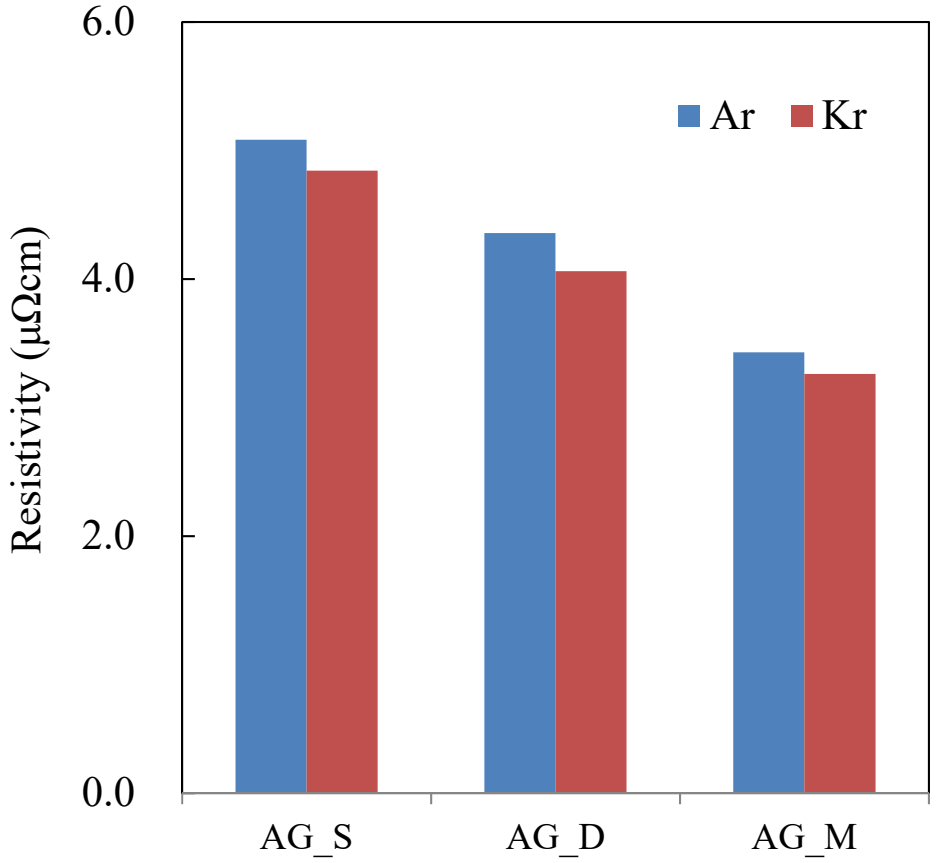

Fig. 4

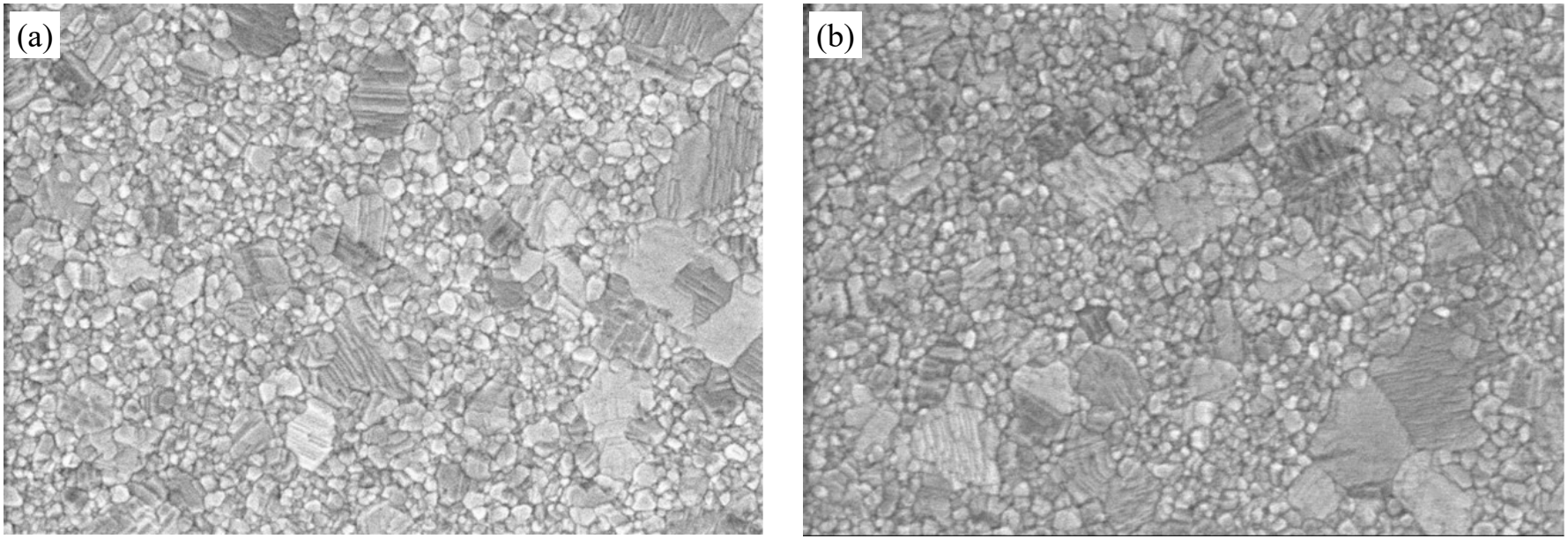
(a)
(b)
Average grain size 55 nm
1.0 µm
Average grain size 58 nm
1.0 µm

Fig. 5

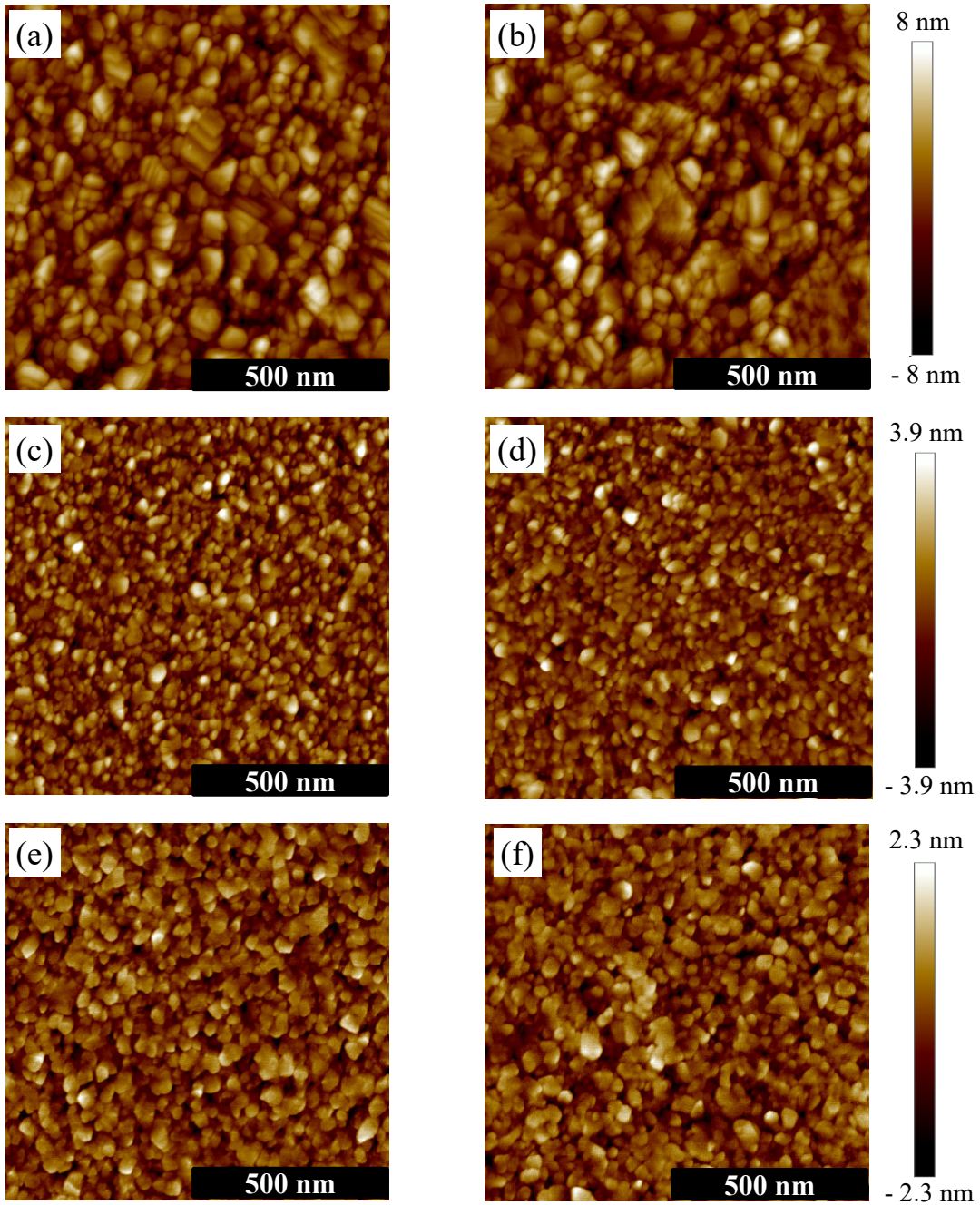
(a)
500 nm
(b)
500 nm
8 nm
- 8 nm
(c)
500 nm
(d)
500 nm
3.9 nm
- 3.9 nm
(e)
500 nm
(f)
500 nm
2.3 nm
- 2.3 nm

Fig. 6

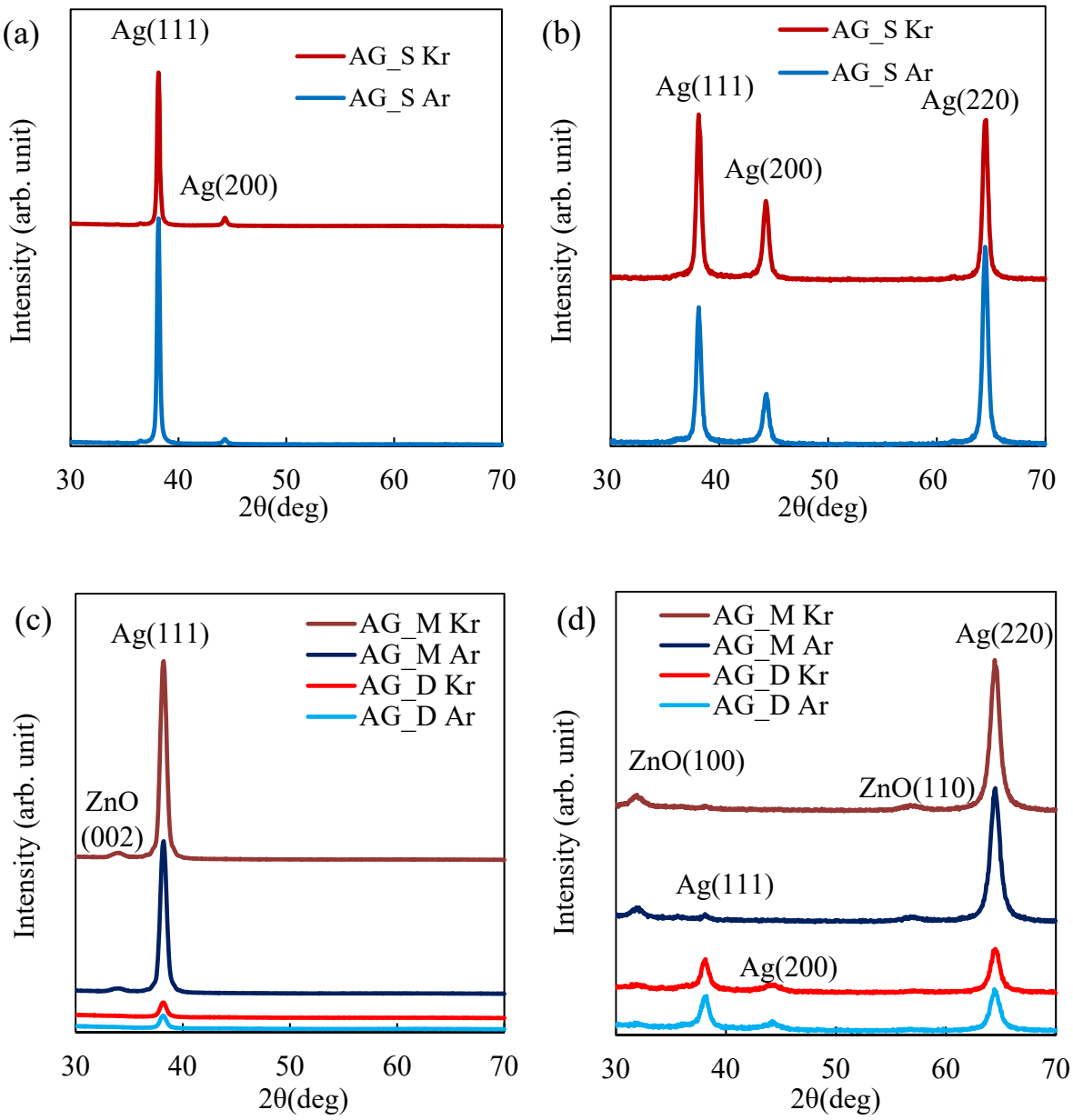
(a)
Ag(111)
AG_S Kr
AG_S Ar
Ag(200)
Intensity (arb. unit)
30
40
50
60
70
2θ(deg)
(b)
AG_S Kr
AG_S Ar
Ag(111)
Ag(220)
Ag(200)
Intensity (arb. unit)
30
40
50
60
70
2θ(deg)
(c)
Ag(111)
AG_M Kr
AG_M Ar
AG_D Kr
AG_D Ar
ZnO
(002)
Intensity (arb. unit)
30
40
50
60
70
2θ(deg)
(d)
AG_M Kr
AG_M Ar
AG_D Kr
AG_D Ar
Ag(220)
ZnO(100)
ZnO(110)
Ag(111)
Ag(200)
Intensity (arb. unit)
30
40
50
60
70
2θ(deg)

Fig. 7

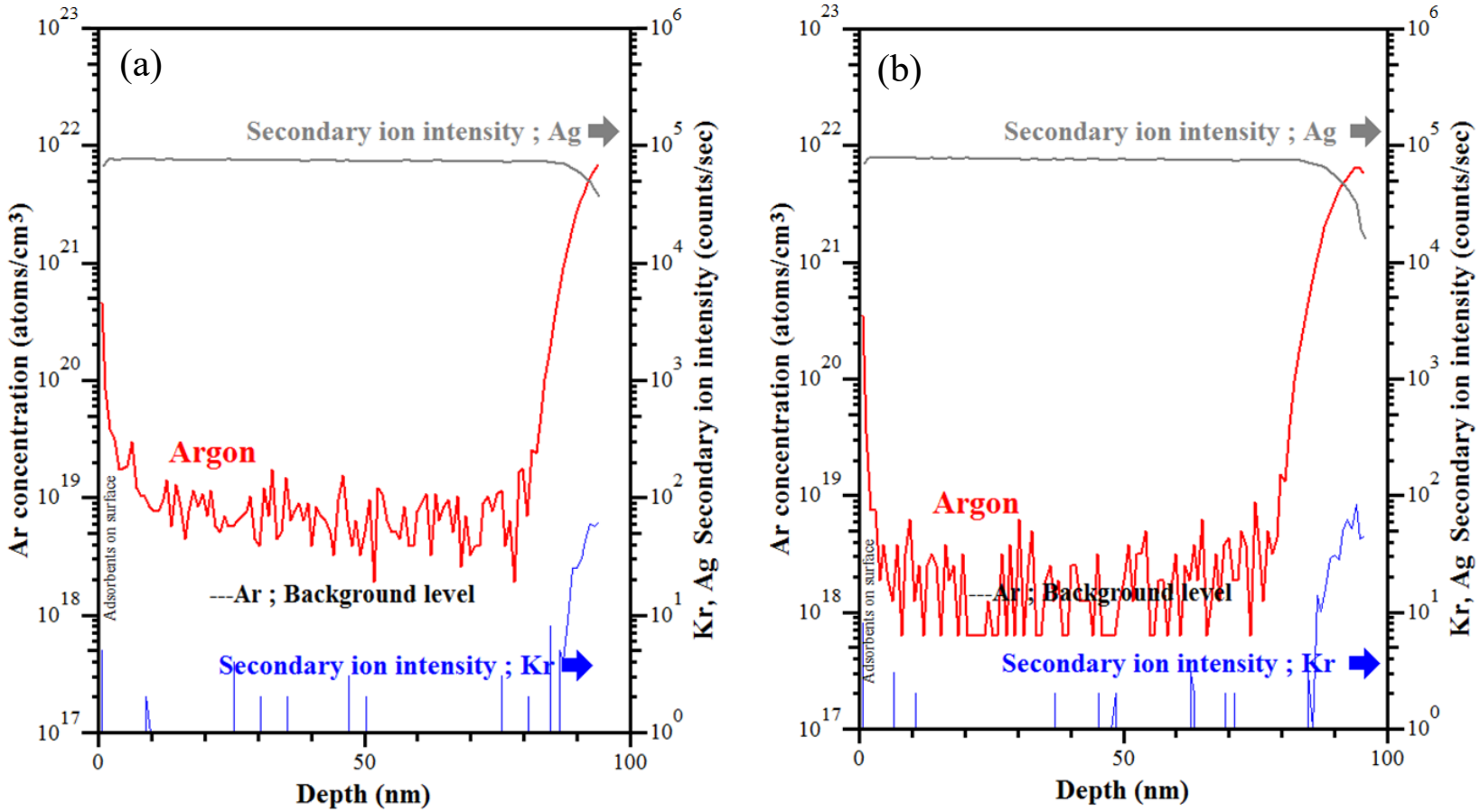
(a)
Secondary ion intensity ; Ag
Argon
---Ar ; Background level
Secondary ion intensity ; Kr
Adsorbents on surface
Ar concentration (atoms/cm3)
Kr, Ag Secondary ion intensity (counts/sec)
Depth (nm)
(b)
Secondary ion intensity ; Ag
Argon
---Ar ; Background level
Secondary ion intensity ; Kr
Adsorbents on surface
Ar concentration (atoms/cm3)
Kr, Ag Secondary ion intensity (counts/sec)
Depth (nm)

Fig. 8